Turkish Journal of Physics

http://journals.tubitak.gov.tr/physics/

Research Article

Turk J Phys
(2020) 44: 288 – 301
© TÜBİTAK
doi:10.3906/fiz-2002-24

Field-free quantum-spin-1/2 XXZ model in three-dimensions: phases, phase transitions, and phase diagrams by renormalization group theory

Ozan S. SARIYER*

Department of Electrical and Electronics Engineering, School of Engineering, Pîrî Reis University, İstanbul, Turkey

Received: 27.02.2020 • **Accepted/Published Online:** 12.04.2020 • **Final Version:** 22.06.2020

Abstract: The field-free quantum-spin-1/2 XXZ model is studied in three-dimensions using renormalization group theory. We obtain global phase diagrams and critical properties. We identify zero-temperature quantum phase transitions at isotropic points, as well as long-range order below critical temperatures at all anisotropies. We show that the excitation spectrum is gapless in XY-like, and gapped in Ising-like anisotropy regimes. Besides, internal energy density, specific heat, nearest-neighbor entanglement measures and spin-spin correlations are obtained globally at all temperatures. Our numerical results cover the global range of anisotropy parameter, for both ferromagnetic and antiferromagnetic cases.

Key words: Statistical mechanics of spin systems, renormalization group theory, thermodynamic functions, quantum entanglement, classical and quantum magnetic phase transitions

1. XXZ model

Quantum magnetic models attract interest, basically due to the possibility of their realizations in information processing systems [1–4], due to their capability of modeling superfluidity [5, 6], and due to the interplay of quantum magnetism and superconductivity [7]. A particular model is the XXZ model, in which the exchange interactions between neighboring spins are uniaxially anisotropic, as defined by the dimensionless Hamiltonian

$$\frac{\mathcal{H}}{kT} = \sum_{\langle ij \rangle} \frac{\mathcal{H}_{ij}}{kT} = -\sum_{\langle ij \rangle} \left[J_x \left(s_i^x s_j^x + s_i^y s_j^y \right) + J_z s_i^z s_j^z \right], \tag{1}$$

where k is the Boltzmann constant, T is the absolute temperature, and the sum is over nearest-neighboring lattice sites. The site-i local operators are equal to one-half the usual Pauli spin operators, $s_i^u \equiv \frac{1}{2}\sigma_i^u$, where u denotes the spin component x, y, or z. The XXZ Hamiltonian operator (1) has the same spectrum for J_x and $-J_x$ [8], which allows us to consider only the $J_x \geqslant 0$ case. Furthermore, the XXZ Hamiltonian operator (1) is symmetric under $x \leftrightarrow y$, which allows us to omit the direction-y, since all physical observables in y-direction are the same as in x-direction, e.g., $\langle s_i^y s_j^y \rangle = \langle s_i^x s_j^x \rangle$ for the nearest-neighbor spin-spin component correlations.

We define a dimensionless temperature as $\frac{T}{\tilde{T}} = \frac{3}{2J_x + |J_z|}$, and a uniaxial anisotropy parameter as $\Delta = \frac{J_z}{J_x}$. The model turns into the classical Ising model for $\Delta \to \pm\infty$, into the isotropic quantum XXX model for $\Delta = \pm 1$, and into the quantum XY model for $\Delta = 0$. These models are ferromagnetic (antiferromagnetic) for $\Delta > 0$ ($\Delta < 0$). The $|\Delta| > 1$ ($|\Delta| < 1$) regime is called the Ising-like (XY-like) regime.

*Correspondence: ossariyer@pirireis.edu.tr

2. Methods

We use an approximate renormalization group (RG) method developed for quantum models by Suzuki and Takano (ST) [9, 10]. The same ST RG method has been applied to quantum lattice gas model [11, 12], Hubbard model [13–16], t-J model [17–20] and Falicov-Kimball model [21]. For the XXZ model, although this approach works best at high temperatures in Ising limits ($T \gg \tilde{T}$, $|\Delta| \gg 1$), previously we demonstrated that even in the opposite zero-temperature XY limit ($T = 0$, $\Delta = 0$), ST RG results obtained for $d = 1$ and $d = 2$, compare well with other approximate results, or with exact results if available. [22, 23] In those work, the details and limitations of the method are discussed elaborately for the XXZ model. In this work, we employ ST RG approach for the hierarchical lattice of real-space rescaling factor $b = 2$ and fractal dimensionality $d = 3$ (see Figure 1). Our results for the FM and AFM Ising models are exact on this hierarchical lattice.

For the XXZ model (1), we consider RG flows in $J_x J_z$-space (see Figure 2), where distinct phases are determined by flows to distinct sink fixed points (see Table 1), and each phase transition is characterized by a critical fixed point (see Table 2). These critical fixed points control the critical exponents and hence the universality class of the transitions.

Besides the phase diagram (see Figure 3) and the critical properties, the main output of an RG method is the expectation values for the operators appearing in the model Hamiltonian, i.e., the nearest-neighbor spin-spin correlations $\langle s_i^x s_j^x \rangle = \langle s_i^y s_j^y \rangle$ and $\langle s_i^z s_j^z \rangle$ for the XXZ model (1). [22, 23] Measures for long-range order and quantum entanglement, as well as internal energy per bond, and thus, heat capacity per bond, can be obtained from the nearest-neighbor spin-spin correlations as follows:

Long-range-order in spin-spin correlations can be identified by using the measure [24–27]

$$\Gamma = \begin{cases} \sqrt{\left|2\,\Delta\,\langle s_i^z s_j^z \rangle\right|} & , |\Delta| \geqslant 1 \\ \frac{2\,\langle s_i^x s_j^x \rangle}{\sqrt{\langle s_i^x s_j^x \rangle + \left|\Delta\,\langle s_i^z s_j^z \rangle\right|}} & , |\Delta| \leqslant 1 \end{cases} . \tag{2}$$

If this measure is greater than a threshold h_d, then spin-spin correlations possess long-range-order. For $d = 3$, a lower bound for h_3 is calculated as $\Gamma_3 \approx 0.350$. [24, 25]

The entanglement of formation $\mathcal{E}$ can be obtained from spin-spin correlations as [28, 29]

$$\mathcal{E} = -g\left[f\left(\mathcal{C}\right)\right] - g\left[1 - f\left(\mathcal{C}\right)\right], \tag{3}$$

where $f\left(\mathcal{C}\right) = \frac{1}{2}\left(1 + \sqrt{1 - \mathcal{C}^2}\right)$, $g\left[f\right] = f \log_2 f$, and the concurrence, being an entanglement monotone, is [29, 30]

$$\mathcal{C} = \max\left[0\,,\, 4\left|\langle s_i^x s_j^x \rangle\right| - \tfrac{1}{2}\left|1 + 4\langle s_i^z s_j^z \rangle\right|\right]. \tag{4}$$

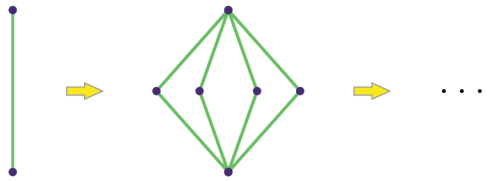

Figure 1. Building step-by-step the $d = 3$ hierarchical lattice suitable for RG of $b = 2$ rescaling factor. At every step, each bond is substituted by four parallel lines ($b^{d-1} = 4$), each containing two bonds ($b = 2$). Repeating such a step infinitely many times, gives a hierarchical lattice, on which our renormalization approach works exact in Ising limits.

The quantum discord $\mathcal{D}$ is another measure of quantum correlations, which can be obtained from nearest-neighbor spin-spin correlations as [29, 31]

$$\mathcal{D} = \frac{1}{4}\Big[g\left(1 - 4\langle s_i^z s_j^z\rangle - 8\langle s_i^x s_j^x\rangle\right) + 2g\left(1 + 4\langle s_i^z s_j^z\rangle\right) + g\left(1 - 4\langle s_i^z s_j^z\rangle + 8\langle s_i^x s_j^x\rangle\right) - 2\left[g_- + g_+\right]\Big], \tag{5}$$

where $g_\pm = g\left(1 \pm 4\max\left[|\langle s_i^x s_j^x\rangle|, |\langle s_i^z s_j^z\rangle|\right]\right)$.

We calculate the dimensionless internal energy per bond $U/\tilde{J}$ as

$$\frac{U}{\tilde{J}} = \frac{\langle \mathcal{H}_{ij}\rangle}{\tilde{J}} = \frac{-3}{2 + |\Delta|}\left(2\langle s_i^x s_j^x\rangle + \Delta\langle s_i^z s_j^z\rangle\right), \tag{6}$$

and the dimensionless heat capacity per bond C/k as

$$\frac{C}{k} = \frac{1}{k}\frac{\partial U}{\partial T} = \frac{\partial(U/\tilde{J})}{\partial(T/\tilde{T})}, \tag{7}$$

where we introduced an energy scale $\tilde{J} = k\tilde{T}$.

3. Results and discussion

3.1. Renormalization group flows, critical points and sinks

RG flows calculated for spatial rescaling factor $b = 2$ and spatial dimensions $d = 3$ is shown in Figure 2, which is in accord with the results of a different RG approximation [32]. For simplicity, we show flows only for $J_z > 0$ and $J_x > 0$. One does not need to consider $J_x < 0$ subspace, due to the symmetry $J_x \leftrightarrow -J_x$ mentioned above. A point in the $J_z < 0$ subspace is renormalized to a point in the $J_z > 0$ subspace in a single RG step, and hence not shown in Figure 2.

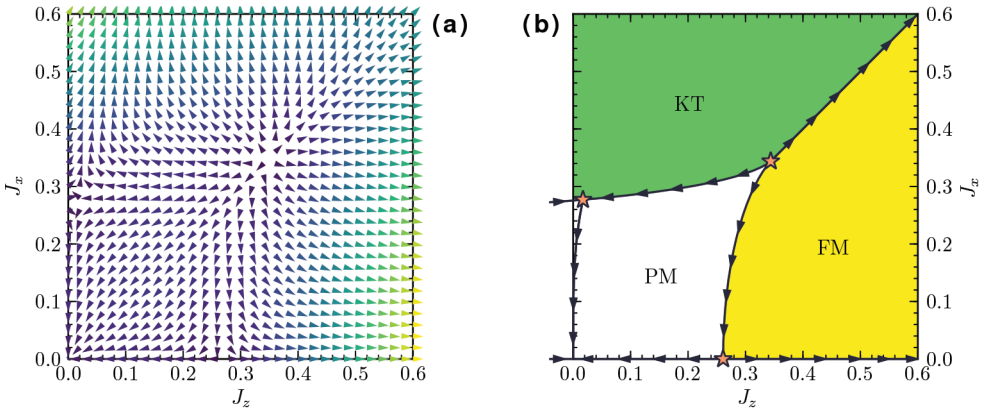

Figure 2. RG flows in the ferromagnetic interactions subspace. In both panels, flow directions are indicated by arrows. **Panel (a):** RG flow field in detail. Flow speed, $\sqrt{(J_x' - J_x)^2 + (J_z' - J_z)^2}$, from fast to slow is coded by colors from yellow to purple. (Primes denote renormalized parameters.) Flows become slower (faster) near (away from) the critical lines. **Panel (b):** Phases, critical fixed points and critical lines. Paramagnetic (PM, white) phase has the infinite-temperature sink at $J_x = 0$, $J_z = 0$; ferromagnetic (FM, yellow) phase has the zero-temperature sink at $J_x = 0$, $J_z \to \infty$; and Kosterlitz-Thouless (KT, green) phase has the zero-temperature sink at $J_x \to \infty$, $J_z \to \infty$ (see Table 1). Shown by star-markers are the XXX, XY and Ising critical fixed points (from top to bottom), which control the universality of phase transitions (see Table 2).

Table 1. Phase sink characteristics: interactions J_u, runaway ratios J'_u/J_u and associated densities $\langle s_i^u s_j^u \rangle$ at sinks.

Sinks	J_z	J_x	J'_z/J_z	J'_x/J_x	$\langle s_i^z s_j^z \rangle$	$\langle s_i^x s_j^x \rangle$
PM	0	0	0	0	0	0
(A)FM	∞	0	4	0	1/4	0
KT	∞	∞	2	2	1/4	0

Table 2. Critical fixed point characteristics: universality classes, interactions J_u^*, and critical exponents in relevant directions y_T at the XXX, XY and Ising critical points, shown in Figure 2(b) as star-markers.

Phase transitions	Universality classes	J_z^*	J_x^*	y_T
(A)FM-PM	Quantum XXX	0.34388	0.34388	0.71516
KT-PM	Quantum XY	0.01706	0.27691	0.86027
(A)FM-PM	Classical Ising	$\pm$0.26107	0	0.93913

Characteristics at sink fixed points are presented in Table 1. Each sink identifies a distinct phase: the disordered paramagnetic (PM) phase at high temperatures, and ordered (anti)ferromagnetic ((A)FM) and Kosterlitz-Thouless (KT) phases at low temperatures. The three stars in Figure 2b denote the critical fixed points, which characterize the phase transitions between different phases. In Table 2, we present the universal characteristics of these critical fixed points. Here, y_T is the relevant scaling exponent at the critical fixed point. [23]

The exponent y_T for the XXX critical point is smaller than the exponent for the XY critical point, and the latter is smaller than the critical exponent for the Ising model as expected [33]. Our calculated values for y_T are to be compared with the values 0.855, 0.917 and 1.15 obtained by Mariz et al. [32], and with 1.39 [34], 1.49 [35] and 1.59 [36] obtained by series expansion, respectively for XXX, XY and Ising critical points in $d = 3$. We note that our results hold for the hierarchical lattice in Figure 1, and that the critical exponents strongly depend on the lattice type.

The critical interaction parameters J_u^* in Table 2 qualitatively agree with the results of Mariz et al.: $J_z^* = J_x^* = 0.239$ for the XXX fixed point, $J_z^* = 0.046$ and $J_x^* = 0.215$ for the XY fixed point, and $J_z^* = 0.183$ and $J_x^* = 0$ for the Ising fixed point [32]. The series expansion results (J_z^*, J_x^*) for XXX, XY and Ising fixed points are respectively $(0.300, 0.300)$ [34], $(0, 0.250)$ [35] and $(0.220, 0)$ [36].

3.2. Phase diagrams

From the RG flows (see Figure 2), we obtain the global phase diagram in $J_z J_x$-space as presented in Figure 3a, and in anisotropy-temperature space as in Figure 3b. For the whole range of anisotropy parameter Δ, there exists phase transitions from the high-temperature disordered paramagnetic PM phase to low-temperature ordered phases: to ferromagnetic FM phase (antiferromagnetic AFM phase) for the Ising-like regime including the isotropic XXX point $\Delta \geqslant 1$ ($\Delta \leqslant -1$), and to a Kosterlitz-Thouless KT phase for the XY-like regime $|\Delta| < 1$. Hence in $d = 3$ dimensions, order-disorder transitions exist at finite-temperatures for the whole range of Δ. We note that this is not the case in $d = 2$ dimensions, where there is no finite-temperature transition for the XXX models at $|\Delta| = 1$ [23]; and in $d = 1$ dimensions, where there is no finite-temperature transition at all [22].

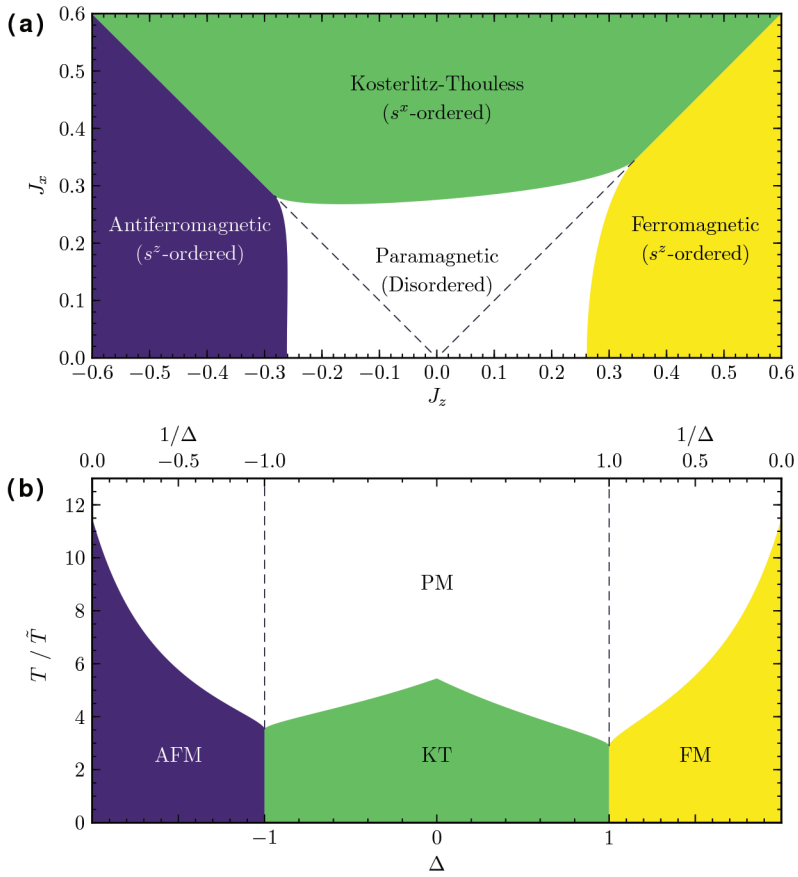

Figure 3. Phase diagrams for the $d = 3$ quantum-spin-$\frac{1}{2}$ XXZ model in dimensionless interactions space **(a)** and in scaled temperature vs. anisotropy space **(b)**. The horizontal axis in panel (b) is chosen as Δ in the XY-like regime, and as $1/\Delta$ in the Ising-like regimes. Dashed lines in both panels are only guides pointing out the isotropic XXX models.

Table 3 shows the critical temperatures $T_c^{(\Delta)}$ for XXX, XY, and Ising models, which involve three-, two-, and one-dimensional spins, respectively. The critical temperature T_c is expected to increase with decreasing spin dimensionality, since it requires less energy kT_c to unsettle the order between higher dimensional spins. We obtain the expected order in critical temperatures, i.e., $T_c^{(\pm 1)} < T_c^{(0)} < T_c^{(\pm\infty)}$. In addition, from Figure 3b, we see that $T_c^{(\Delta)}$ falls off as absolute anisotropy $|\Delta|$ is scanned either from Ising models ($1d$ spins) or from XY model ($2d$ spins) to XXX models ($3d$ spins). These expected trends were also obtained by other RG approximations for cubic lattices [32, 37–40], with qualitative agreement to our phase diagrams of Figure 3.

Table 3. Dimensionless critical temperatures, $T_c^{(\Delta)}/\tilde{T} = 3/(2J_x^c + |J_z^c|)$, and dimensionless interactions, J_u^c, for XXX, XY and Ising models. Critical temperature increases with decreasing spin dimensionality as expected.

Models	Spin dimensions	Critical temperatures	Critical interactions
FM XXX ($\Delta = 1$, $J_x = J_z$)	3	$T_c^{(1)}/\tilde{T} = 2.907958$	$J_x^c = J_z^c = 0.343884$
AFM XXX ($\Delta = -1$, $J_x = \|J_z\|$)	3	$T_c^{(-1)}/\tilde{T} = 3.541227$	$J_x^c = -J_z^c = 0.282388$
XY ($\Delta = 0$, $J_z = 0$)	2	$T_c^{(0)}/\tilde{T} = 5.444572$	$J_x^c = 0.275504$
(A)FM Ising ($\|\Delta\| \to \infty$, $J_x = 0$)	1	$T_c^{(\pm\infty)}/\tilde{T} = 11.491383$	$\|J_z^c\| = 0.261065$

We also note a quantum mechanically induced asymmetry between critical temperatures of AFM-PM and FM-PM transitions, i.e., $T_c^{(-\Delta)}/T_c^{(\Delta)} > 1$ for positive Δ, as plotted in Figure 4. The critical temperatures ratio, $T_c^{(-\Delta)}/T_c^{(\Delta)}$, is unity only for XY and Ising models, but is maximal for the XXX model. Our result for the peak, $T_c^{(-1)}/T_c^{(1)} = 1.21777$, compares well with the results 1.48 [41], 1.22 [16, 17], 1.13 [42], 1.12 [43–45], 1.11 [46], 1.10 and 1.08 [47] obtained for $d = 3$ by various methods.

3.3. Long-range-order measure

Figure 5 shows our results for the long-range-order measure Γ [see equation (2)] in anisotropy-temperature space. The contour plot is clipped at $\Gamma = 2.2$, for Γ growing fast close to Ising models at low temperatures. We have a region of $\Gamma > \Gamma_3$ at low temperatures for all Δ, where $\Gamma_3 \approx 0.350$ is the estimated long-range-order threshold lower bound. [24, 25]

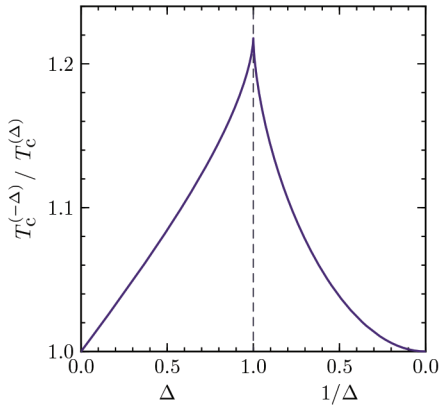

Figure 4. The ratio of AFM critical temperature $T_c^{(-\Delta)}$ to FM critical temperature $T_c^{(\Delta)}$ with the same absolute anisotropy, plotted as a function of Δ and $1/\Delta$ in XY-like and Ising-like regimes respectively.

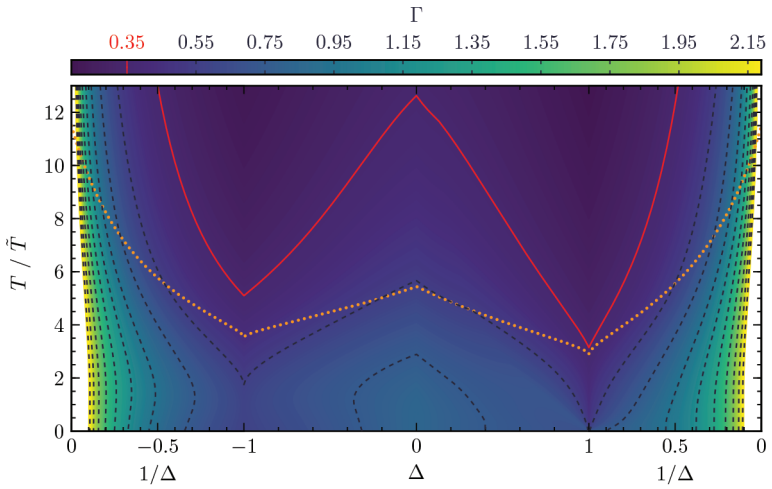

Figure 5. Contour plot of long-range-order measure Γ in anisotropy-temperature space. The horizontal axis is chosen as Δ ($1/\Delta$) in XY-like (Ising-like) regime. Solid red contour marks the estimated long-range-order threshold lower bound, $\Gamma_3 \approx 0.350$. Order-disorder phase transition lines (see Figure 3(b)) are superimposed as the orange dotted line.

In the same Figure 5, we also superpose the order-disorder phase transition lines (orange dotted lines, see Figure 3b). We observe that the approximate critical temperature of long-range order obtained from $\Gamma(\Delta, T_c^{(\Delta)}) = \Gamma_3$ overestimates the real critical temperature for the whole range of anisotropy. Nonetheless, we can qualitatively conclude that the low-temperature ordered (A)FM and KT phases exhibit log-range order.

3.4. Excitation spectrum gap at low-temperatures

In Appendix, we present global results for spin-spin correlations ($\langle s_i^x s_j^x \rangle$ and $\langle s_i^z s_j^z \rangle$) as well as other thermodynamic functions obtained from the spin-spin correlations. These functions are entanglement of formation ($\mathcal{E}$), quantum discord ($\mathcal{D}$), dimensionless internal energy per bond ($U/\tilde{J}$), and dimensionless heat capacity per bond (C/k). We observe that low-temperature behavior of specific heat is different in XY-like and Ising-like regimes, see Figure 10d.

In both the AFM and FM phases of the Ising-like regime, there exist a gap between the ground-state and the thermally excited states. This exication gap results in exponential specific heat vs. temperature behavior at low-T. On the other hand, the KT phase of the XY-like regime is a spin-liquid phase, and the excitations from the ground-states are gapless, resulting in a specific heat that is linear in temperature at low-T: $C = \gamma_0 T$, where γ_0 is the Sommerfeld coefficient. [22, 23]

In Figure 6a, we plot the dimensionless heat capacity per bond as a function of temperature at low-T, for a variety of anisotropies in the range $-1 \leq \Delta \leq 1$. We observe the expected linear behavior. Here, we define a dimensionless Sommerfeld coefficient as

$$\frac{\gamma_0}{k/\tilde{T}} = \lim_{T \to 0} \frac{C/k}{T/\tilde{T}}, \tag{8}$$

and plot the results for it in Figure 6b, where we observe that the dimensionless Sommerfeld coefficient is zero for AFM XXX model; increases with increasing anisotropy parameter; and falls discontinuously to zero at FM XXX model. The Sommerfeld coefficient persists at zero in both AFM and FM Ising-like regimes. Hence, we resolve that the low-temperature excitations in the XY-like regime are gapless, while in the Ising-like regimes an excitation gap exists.

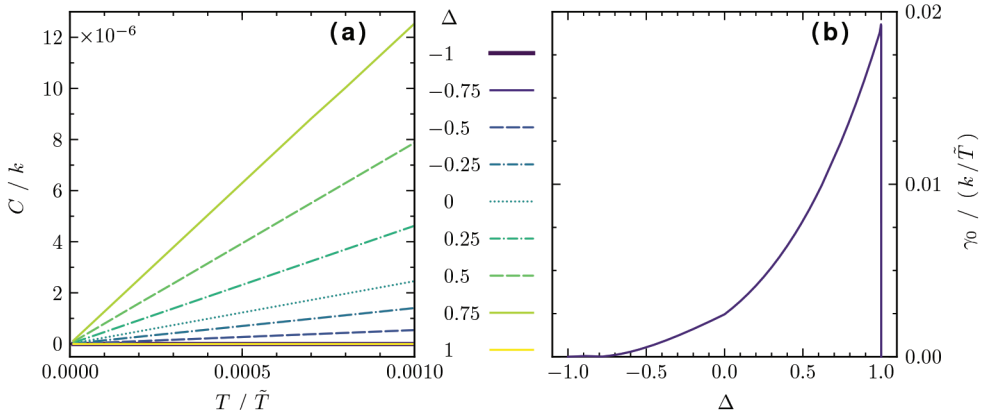

Figure 6. **Panel (a):** Scaled specific heat C/k plotted as a function of scaled temperature $T/\tilde{T}$, for various Δ in the XY-like regime as indicated in the legend. Note the factor of 10^{-6} for the vertical axis. **Panel (b):** Scaled Sommerfeld coefficient $\gamma_0 \tilde{T}/k$ plotted as a function of anisotropy parameter Δ in the XY-like regime, $-1 \leqslant \Delta \leqslant 1$.

3.5. Quantum phase transitions at zero-temperature

To identify the quantum phase transitions between ordered KT and (A)FM phases (see Figure 2), we calculated the thermodynamic and entanglement functions at zero-temperature: spin-spin correlations $\langle s_i^x s_j^x \rangle_0$ and $\langle s_i^z s_j^z \rangle_0$, scaled internal energy per bond $U_0/\tilde{J}$, and entanglement functions $\mathcal{C}_0$, $\mathcal{E}_0$ and $\mathcal{D}_0$, which are plotted as functions of anisotropy in Figure 7. Here, the 0-subscripts are used to denote $T = 0$.

The cusp peak in $U_0/\tilde{J}$, and the jumps in $\langle s_i^x s_j^x \rangle_0$, $\langle s_i^z s_j^z \rangle_0$, $\mathcal{C}_0$, $\mathcal{E}_0$ and $\mathcal{D}_0$, are due to the discontinuous KT-FM quantum phase transition at $\Delta = 1$, while the local maxima in $U_0/\tilde{J}$, $\mathcal{C}_0$ and $\mathcal{E}_0$ are due to the continuous AFM-KT quantum phase transition at $\Delta = -1$. [22, 23, 30, 48, 49]

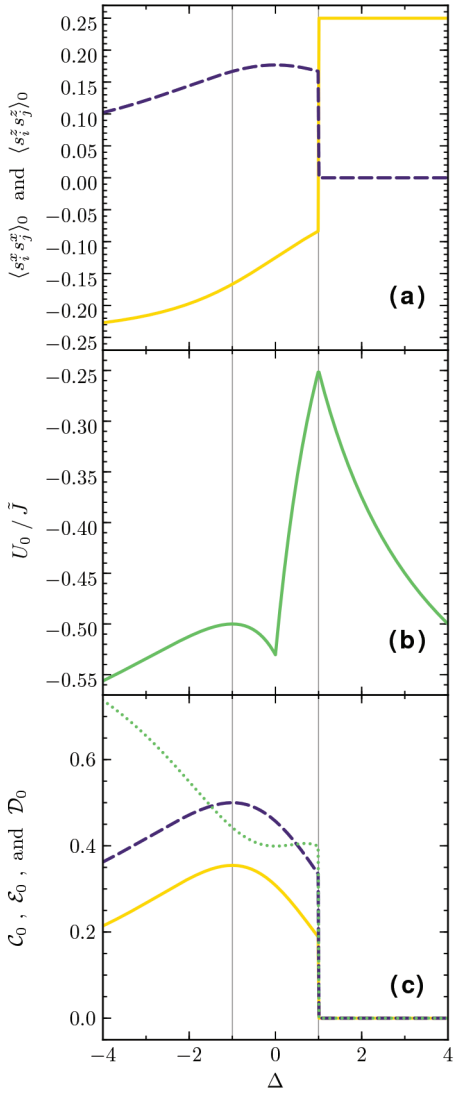

Figure 7. Thermodynamic and entanglement functions at zero-temperature as functions of anisotropy parameter. **Panel (a):** spin-spin correlations $\langle s_i^z s_j^z \rangle_0$ (solid yellow) and $\langle s_i^x s_j^x \rangle_0$ (dashed purple). **Panel (b):** scaled internal energy per bond $U/\tilde{J}$ (solid green). **Panel (c):** concurrence $\mathcal{C}_0$ (dashed purple), entanglement of formation $\mathcal{E}_0$ (solid yellow), and quantum discord $\mathcal{D}_0$ (dotted green). Thin vertical lines are guides to show isotropic XXX points, $\Delta = \pm 1$.

Acknowledgment

I would like to thank Prof. Dr. A. Nihat BERKER (Faculty of Engineering and Natural Sciences, Kadir Has University, İstanbul, Turkey) for suggesting this problem to me. A machine partially supported by The Scientific and Technological Research Council of Turkey (TÜBİTAK) under 2232 Reintegration Grant # 115C135 was used for numerical calculations.

References

[1] Loss D, Di Vincenzo DP. Quantum computation with quantum dots. Physical Review A 1998; 51 (1): 120-126. doi: 10.1103/PhysRevA.57.120

[2] Burkard G, Loss D, Di Vincenzo DP. Coupled quantum dots as quantum gates. Physical Review B 1999; 59 (3): 2070-2078. doi: 10.1103/PhysRevB.59.2070

[3] Glaser U, Büttner H, Fehske H. Entanglement and correlation in anisotropic quantum spin systems. Physical Review A 2003; 68 (3): 032318–1-8. doi: 10.1103/PhysRevA.68.032318

[4] Amico L, Fazio R, Osterloh A, Vedral V. Entanglement in many-body systems. Reviews of Modern Physics 2008; 80 (2): 517-576. doi: 10.1103/RevModPhys.80.517

[5] Matsubara T, Matsuda H. A lattice model of liquid helium, I. Progress of Theoretical Physics 1956; 16 (6): 569-582. doi: 10.1143/PTP.16.569

[6] Matsuda H, Matsubara T. A lattice model of liquid helium, II. Progress of Theoretical Physics 1957; 17 (1): 19-29. doi: 10.1143/PTP.17.19

[7] Anderson PW. The resonating valence bond state in La_2CuO_4 and superconductivity. Science 1987; 235 (4793): 1196-1198. doi: 10.1126/science.235.4793.1196

[8] Yang CN, Yang CP. Ground-state energy of a Heisenberg-Ising lattice. Physical Review 1966; 147 (1): 303-306. doi: 10.1103/PhysRev.147.303

[9] Suzuki M, Takano H. Migdal renormalization group approach to quantum spin systems. Physics Letters A 1979; 69 (6): 426-428. doi: 10.1016/0375-9601(79)90397-9

[10] Takano H, Suzuki M. Migdal-Kadanoff renormalization group approach to the spin-1/2 anisotropic Heisenberg model. Journal of Statistical Physics 1981; 26 (4): 635-663. doi: 10.1007/BF01010931

[11] Sano K, Doi I, Minoguchi T. The superfluid transition of ^{4}He in zeolite by the quantum lattice gas model. Japanese Journal of Applied Physics 1987; 26 (Supplement 26-3, Part 1): 291-292. doi: 10.7567/JJAPS.26S3.291

[12] Doi I. The superfluid transition of ^{4}He adsorbed in zeolite —A theoretical study based on the quantum lattice gas model—. Journal of the Physical Society of Japan 1989; 58 (4): 1312-1319. doi: 10.1143/JPSJ.58.1312

[13] Cannas SA, Tamarit FA, Tsallis C. A generalised Hubbard Hamiltonian: influence of temperature and fractality. Solid State Communications 1991; 78 (8): 685-690. doi: 10.1016/0038-1098(91)90845-M

[14] Cannas SA, Tamarit FA, Tsallis C. Generalised Hubbard Hamiltonian: renormalization-group approach. Physical Review B 1992; 45 (18): 10496-10508. doi: 10.1103/PhysRevB.45.10496

[15] Migliorini G, Berker AN. Finite-temperature phase diagram of the Hubbard model. The European Physical Journal B 2000; 17 (1): 3-6. doi: 10.1007/s100510070153

[16] Hinczewski M, Berker AN. Two superconducting phases in the $d = 3$ Hubbard model. The European Physical Journal B 2005; 48 (1): 1-17. doi: 10.1140/epjb/e2005-00376-y

[17] Falicov A, Berker AN. Finite-temperature phase diagram of the t-J model: renormalization-group theory. Physical Review B 1995; 51 (18): 12458-12463. doi: 10.1103/PhysRevB.51.12458

[18] Hinczewski M, Berker AN. $d = 3$ anisotropic and $d = 2$ tJ models: phase diagrams, thermodynamic properties, and chemical potential shift. The European Physical Journal B 2006; 51 (4): 461-472. doi: 10.1140/epjb/e2006-00258-x

[19] Hinczewski M, Berker AN. Finite-temperature phase diagram of nonmagnetic impurities in high-temperature superconductors using a $d = 3$ tJ model with quenched disorder. Physical Review B 2008; 78 (6): 064507–1-5. doi: 10.1103/PhysRevB.78.064507

[20] Kaplan CN, Berker AN, Hinczewski M. Frustrated further-neighbor antiferromagnetic and electron-hopping interactions in the $d = 3$ t-J model: Finite-temperature global phase diagrams from renormalization group theory. Physical Review B 2009; 80 (21): 214529–1-11. doi: 10.1103/PhysRevB.80.214529

[21] Sarıyer OS, Hinczewski M, Berker AN. Phase separation and charge-ordered phases of the $d = 3$ Falicov-Kimball model at nonzero temperature: Temperature-density-chemical potential global phase diagram from renormalization-group theory. Physical Review B 2011; 84 (20): 205120–1-13. doi: 10.1103/PhysRevB.84.205120

[22] Sarıyer OS, Berker AN, Hinczewski M. Excitation spectrum gap and spin-wave velocity of XXZ Heisenberg chains: Global renormalization-group calculation. Physical Review B 2008; 77 (13): 134413–1-10. doi: 10.1103/PhysRevB.77.134413

[23] Sarıyer OS. Two-dimensional quantum-spin-1/2 XXZ magnet in zero magnetic field: Global thermodynamics from renormalisation group theory. Philosophical Magazine 2019; 99 (14): 1787-1824. doi: 10.1080/14786435.2019.1605212

[24] Kubo K, Kishi T. Existence of long-range order in the XXZ model. Physical Review Letters 1988; 61 (22): 2585-2587. doi: 10.1103/PhysRevLett.61.2585

[25] Ozeki Y, Nishimori H, Tomita Y. Long-range order in antiferromagnetic quantum spin systems. Journal of the Physical Society of Japan 1989; 58 (1): 82-90. doi: 10.1143/JPSJ.58.82

[26] Nishimori H, Ozeki Y. Ground-state long-range order in the two-dimensional XXZ model. Journal of the Physical Society of Japan 1989; 58 (3): 1027-1030. doi: 10.1143/JPSJ.58.1027

[27] Wischmann HA, Müller-Hartmann E. Extended proof of long-range order in the two-dimensional quantum spin-1/2 XXZ-model at $T = 0$. Journal de Physique I 1991; 1 (5): 647-657. doi: 10.1051/jp1:1991109

[28] Fanchini FF, Werlang T, Brasil CA, Arruda LGE, Caldeira AO. Non-Markovian dynamics of quantum discord. Physical Review A 2010; 81 (5): 052107–1-6. doi: 10.1103/PhysRevA.81.052107

[29] Werlang T, Trippe C, Ribeiro GAP, Rigolin G. Quantum correlations in spin chains at finite temperatures and quantum phase transitions. Physical Review Letters 2010; 105 (9): 095702–1-4. doi: 10.1103/PhysRevLett.105.095702

[30] Justino L, de Oliveira TR. Bell inequalities and entanglement at quantum phase transitions in the XXZ model. Physical Review A 2012; 85 (5): 052128–1-7. doi: 10.1103/PhysRevA.85.052128

[31] Luo S. Quantum discord for two-qubit systems. Physical Review A 2008; 77 (4): 042303–1-6. doi: 10.1103/PhysRevA.77.042303

[32] Mariz AM, Zorzenon Dos Santos RM, Tsallis C, Dos Santos RR. Critically of the anisotropic quantum Heisenberg model on a simple cubic lattice. Physics Letters A 1985; 108 (2): 95-98. doi: 10.1016/0375-9601(85)90525-0

[33] Suzuki M. Dependence of critical exponents upon symmetry, dimensionality, potential-range and strength of interaction. Physics Letters A 1972; 38 (1): 23-24. doi: 10.1016/0375-9601(72)90958-9

[34] Rushbrooke GS, Baker Jr GA, Wood PJ. Heisenberg model. In: Domb C, Green MS (editors). Phase Transitions and Critical Phenomena. Vol. 3. New York, NY, USA: Academic Press, 1974, pp. 246-356.

[35] Betts DD. X-Y model. In: Domb C, Green MS (editors). Phase Transitions and Critical Phenomena. Vol. 3. New York, NY, USA: Academic Press, 1974, pp. 570-652.

[36] Domb C. Ising model. In: Domb C, Green MS (editors). Phase Transitions and Critical Phenomena. Vol. 3. New York, NY, USA: Academic Press, 1974, pp. 357-485.

[37] Plascak JA. Quantum spin systems: dynamical mean field renormalisation group approach. Journal of Physics A: Mathematical and General 1984; 17 (13): L597-L600. doi: 10.1088/0305-4470/17/13/004

[38] Lee F, Chen HH, Tseng HC. Preservation of the free energy in a Migdal-Kadanoff approximation for the spin-1/2 anisotropic Heisenberg model. Physical Review B 1988; 37 (10): 5371-5374. doi: 10.1103/PhysRevB.37.5371

[39] Lee F, Chen HH, Tseng HC. Modified Migdal-Kadanoff renormalization for the spin-$\frac{1}{2}$ anisotropic Heisenberg model. Physical Review B 1988; 38 (1): 508-511. doi: 10.1103/PhysRevB.38.508

[40] Ricardo de Sousa J, Fittipaldi IP. Critical behavior of the anisotropic Heisenberg model by effective-field renormalization group. Journal of Applied Physics 1994; 75 (10): 5835-5837. doi: 10.1063/1.355584

[41] Kaplan CN, Berker AN. Quantum-mechanically induced asymmetry in the phase diagrams of spin-glass systems. Physical Review Letters 2008; 100 (2): 027204–1-4. doi: 10.1103/PhysRevLett.100.027204

[42] Oitmaa J, Zheng W. Curie and Néel temperatures of quantum magnets. Journal of Physics: Condensed Matter 2004; 16 (47): 8653-8660. doi: 10.1088/0953-8984/16/47/016

[43] Rushbrooke GS, Wood PJ. On the high temperature staggered susceptibility of Heisenberg model antiferromagnetics. Molecular Physics: An International Journal at the Interface Between Chemistry and Physics 1963; 6 (4): 409-421. doi: 10.1080/00268976300100461

[44] Charles Jr HK, Joseph RI. Critical properties of antiferromagnets. Physical Review Letters 1972; 28 (13): 823-825. doi: 10.1103/PhysRevLett.28.823

[45] Kasteleijn PW, Van Kranendonk J. Constant coupling approximation for Heisenberg ferromagnetism. Physica (Utrecht) 1956; 22 (1-5): 317-337. doi: 10.1016/S0031-8914(56)80044-X ; ibid. Constant coupling approximation for antiferromagnetism. 367-385. doi: 10.1016/S0031-8914(56)80051-7

[46] Mano H. Study of critical phenomena of quantum spin systems by spin-cluster approximation series. Journal of Magnetism and Magnetic Materials 1990; 90-91: 281-283. doi: 10.1016/S0304-8853(10)80100-3

[47] Li YY. Application of the Bethe-Weiss method to the theory of antiferromagnetism. Physical Review 1951; 84 (4): 721-730. doi: 10.1103/PhysRev.84.721

[48] Braiorr-Orrs B, Weyrauch M, Rakov MV. Numerical studies of entanglement properties in one- and two-dimensional quantum Ising and XXZ models. Ukrainian Journal of Physics 2016; 61 (7): 613-626. doi: 10.15407/ujpe61.07.0613

[49] Bishop RF, Farnell DJJ, Parkinson JB. The coupled-cluster method applied to the XXZ model using a planar model state. Journal of Physics: Condensed Matter 1996; 8 (50): 11153-11165. doi: 10.1088/0953-8984/8/50/038

Appendix

Here we provide global numerical results for various thermodynamic and entanglement functions: nearest-neighbor spin-spin correlations $\langle s_i^z s_j^z \rangle$ and $\langle s_i^x s_j^x \rangle$ in Figure 8, quantum entanglement measures $\mathcal{E}$ and $\mathcal{D}$ in Figure 9, and finally, thermodynamic functions $U/\tilde{J}$ and C/k in Figure 10. In all these Figures, in panels (a) and (b), we show contour plots for these physical quantities as functions of anisotropy parameter and scaled temperature, and in panels (c) and (d) we plot them as functions of temperature for a variety of anisotropy parameters covering the global range from AFM to FM Ising limits, as indicated in the legends. The horizontal axes in panels (a) and (b) are chosen as Δ in the XY-like regime, and as $1/\Delta$ in the Ising-like regimes. We note that these functions show the same qualitative behavior (e.g., same discontinuous jumps, cusps, maxima, peaks and double peaks), as in one- and two-dimensional models discussed in detail previously. [22, 23]

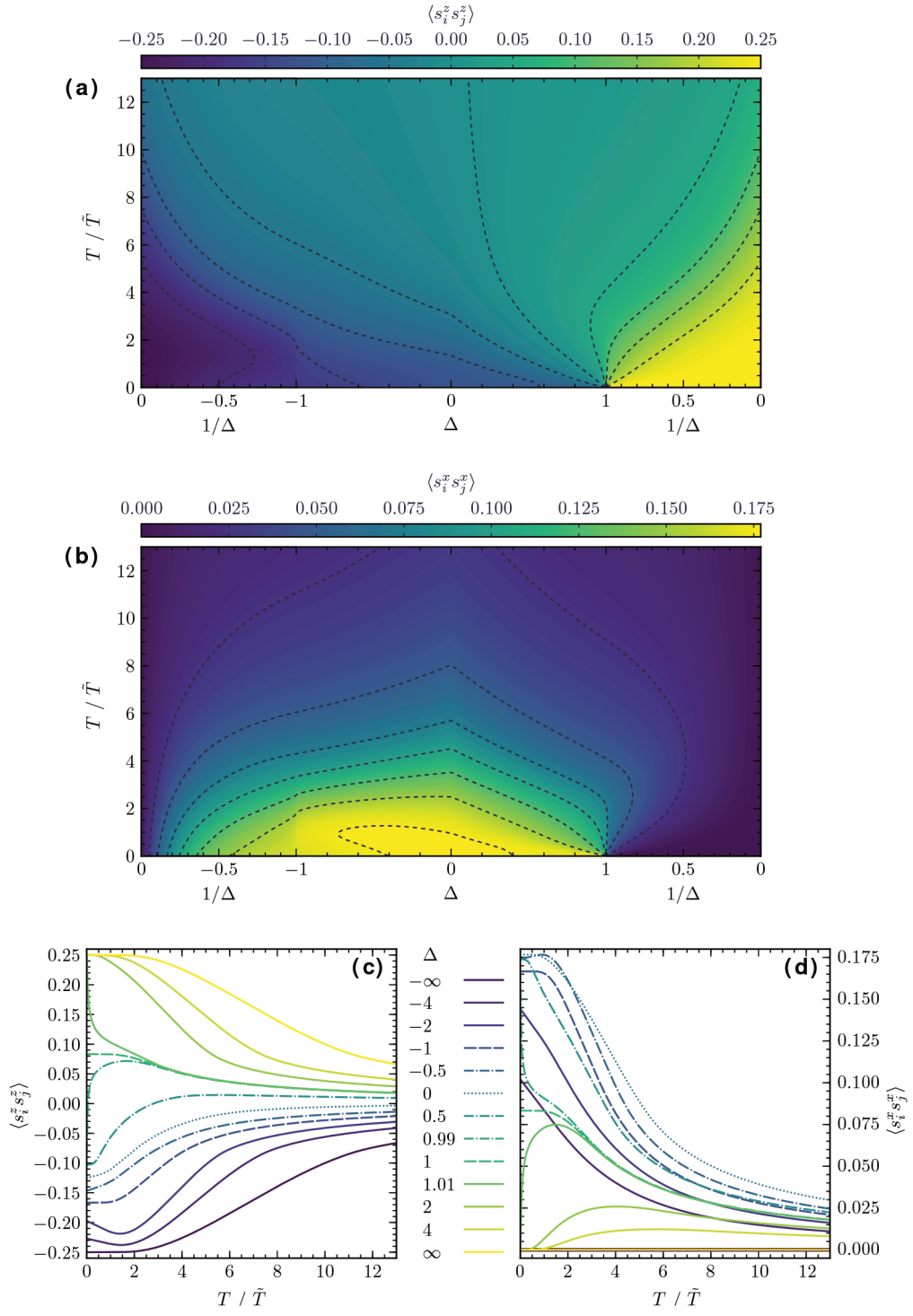

Figure 8. Nearest-neighbor spin-spin correlations $\langle s_i^z s_j^z \rangle$ **(a)(c)** and $\langle s_i^x s_j^x \rangle$ **(b)(d)**.

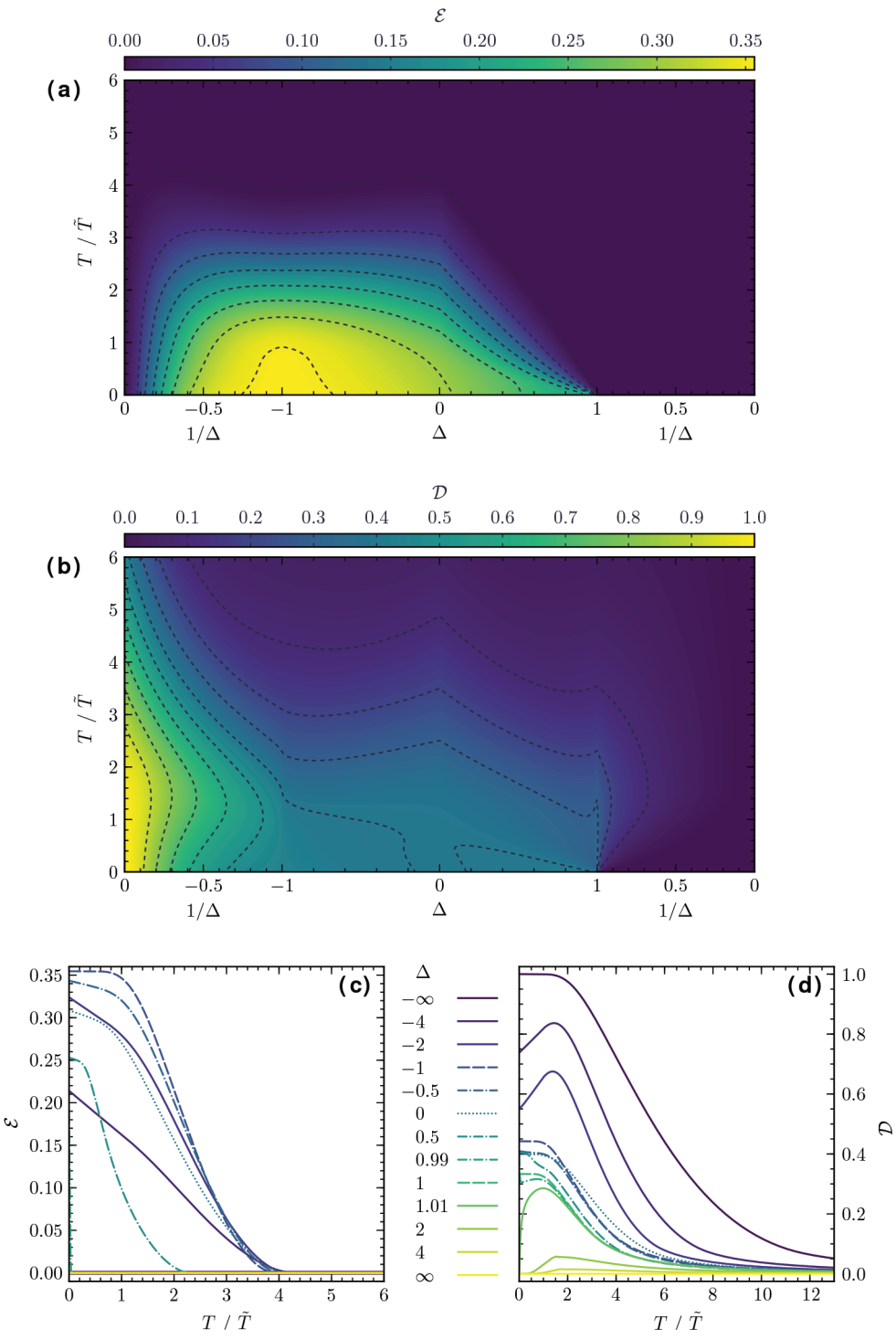

Figure 9. Entanglement of formation $\mathcal{E}$ **(a)(c)** and quantum discord $\mathcal{D}$ **(b)(d)**.

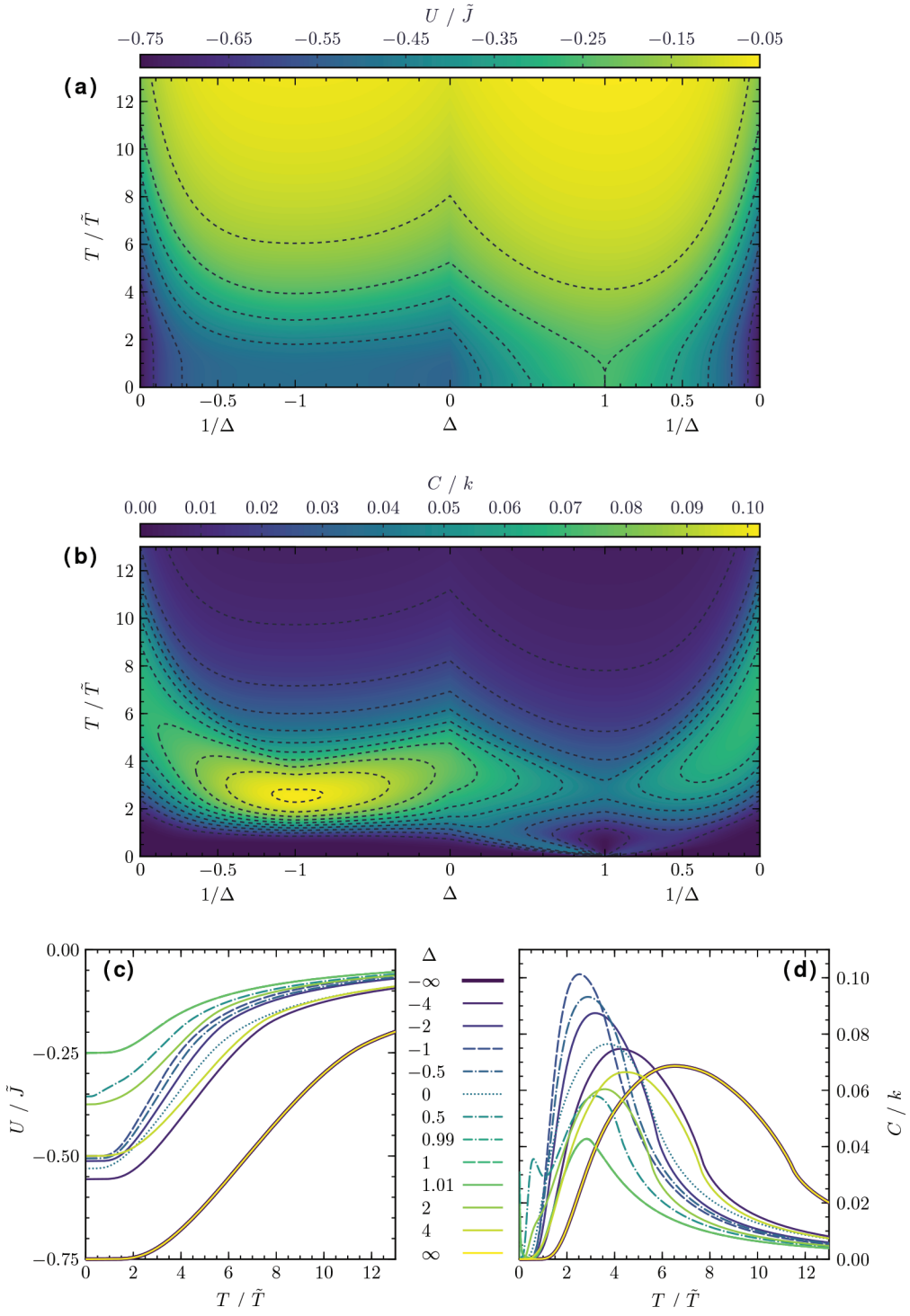

Figure 10. Dimensionless internal energy per bond $U/\tilde{J}$ **(a)(c)** and dimensionless heat capacity per bond C/k **(b)(d)**.